Journal of Electron Spectroscopy and Related Phenomena xxx (2014) xxx–xxx

Contents lists available at ScienceDirect

Journal of Electron Spectroscopy and Related Phenomena

journal homepage: www.elsevier.com/locate/elspec

Future directions in standing-wave photoemission

Alexander X. Gray*

Department of Physics, Temple University, Philadelphia, PA 19122, USA

ARTICLE INFO

Article history:
Available online xxx

Keywords:
Photoelectron spectroscopy
Standing-waves
X-ray optics
Electronic structure
Interface phenomena

ABSTRACT

Over the past decade, standing-wave photoemission (SW-XPS) has evolved into a powerful and versatile non-destructive technique for probing element-specific electronic, magnetic, and structural properties of buried layers and interfaces with sub-nanometer depth resolution. In this article, I will discuss several promising future directions in this emergent field stemming from experimental and theoretical studies wherein SW-XPS is combined with other X-ray techniques, such as magnetic circular dichroism (MCD), hard X-ray photoemission spectroscopy (HAXPES), angle-resolved photoemission (ARPES), and photoemission microscopy (PEEM), adding extra dimensions to the measurement and thus widening the scope of scientific and technological questions accessible via the use of standing waves. I will further discuss examples of recently developed methods for X-ray standing-wave data analysis, which yield layer-resolved matrix-element-weighted densities of states at interfaces as well as Ångstrom-level changes in periodicity of synthetic superlattices. Finally, I will explore the possibility of localizing the standing waves near the surface and within a buried layer by the use of aperiodic superlattices, total reflection, and X-ray waveguide effects.

1. Introduction

X-ray photoelectron spectroscopy (XPS) is a powerful and well-established experimental technique for probing the electronic structure and chemical composition of matter. The key physical phenomenon behind photoemission, the photoelectric effect, was first understood and explained by Einstein in 1905, which earned him a Nobel Prize in Physics in 1921 [1]. It was not until the late 1950s, however, that the true potential of this effect was discovered by Kai Siegbahn who utilized photoemission for studying the composition and electronic properties of solids, which resulted in another Nobel Prize in 1981 [2].

Over the next five decades since the first experiments in Uppsala [3,4], the field of photoemission has undergone tremendous advances both in the realms of powerful new instrumentation and advanced theoretical machinery for interpreting and modeling experimental results. Perhaps one of the most important leaps forward happened with the advent of synchrotron light sources, allowing continuous tuning of the excitation energy over the range of hundreds of eV in the soft X-ray regime and several keV in the hard X-ray regime [5]. This advance has stimulated development of new experimental X-ray techniques, which add new dimensions to the traditional photoemission spectroscopy. Among such techniques are photoelectron microscopy (PEEM) for spatially resolved element-specific nanoscale imaging [6–8], angle-resolved photoelectron spectroscopy (ARPES) for momentum-resolved valence electronic structure band-mapping [9,10], and X-ray photoelectron diffraction (XPD) and holography for element-specific surface structure determination [11,12]. All of the above-mentioned techniques take full advantage of extremely useful features of synchrotron radiation such as variable polarization – which allows probing of element-specific ferro- and antiferromagnetic structure [13–15] and orbital polarization [16,17] via X-ray magnetic circular and linear dichroism (XMCD and XMLD) – as well as the ability to tune the photon energy to core-level resonances in order to enhance the signal from a specific element [18,19].

Despite its tremendous success as a powerful and versatile characterization technique, photoemission has earned the reputation of being an inherently surface-sensitive probe due to the short inelastic mean-free paths (IMFP) of photoelectrons in solids. The widely used TPP-2 M formula, which yields estimated values of effective attenuation lengths for most solids with reasonable accuracy, predicts typical IMFPs of 3–25 Å for the photoemitted electrons with kinetic energies between 50 and 1500 eV (standard soft X-ray XPS regime) [20,21]. Motivated by this shortcoming, and enabled by the development of third-generation synchrotron undulators [22], high-resolution hard X-ray monochromators [23] and high-throughput electron analyzers tuned specifically for highly energetic photoelectrons [24], synchrotron-based

* Tel.: +1 5105126776.
E-mail address: axgray@temple.edu

http://dx.doi.org/10.1016/j.elspec.2014.05.004
0368-2048/

photoemission leaped into the hard X-ray regime (2–15 keV) taking advantage of roughly a 4–20 fold increase of the average probing depth [25]. Since the seminal experiments in the mid-2000s [26], hard X-ray photoemission (HAXPES) has firmly planted its roots at several synchrotron facilities around the world [27] and researchers have successfully combined HAXPES with photoelectron microscopy (HAXPEEM) [28], angle-resolved photoemission (HARPES) [29,30], and magnetic circular dichroism [31].

Yet, even at higher photon energies, the photoemission signal originating closer to the surface will always dominate over the signal originating from below according to $I(Z) = I_0 \exp[-z/\Lambda \sin\theta_{TOA}]$, where z is the depth, Λ is the IMFP, and θ_{TOA} is the electron takeoff angle relative to the surface [32]. Such constraint makes it difficult or, most of the time, impossible to use conventional soft- and hard X-ray photoemission for extracting electronic structure information from the layers and/or interfaces that are buried within a multilayer film structure or a device, particularly if the overlayers have a similar atomic composition as the buried layer/interface of interest. This limitation can, however, be circumvented by tailoring the intensity profile of the electromagnetic field of the incident X-ray radiation inside the sample in such a way as to highlight the regions of the sample which are buried beneath the surface while suppressing photoemission from the overlayer. Such controllable depth selectivity in an experiment can be accomplished by the technique called standing-wave photoemission spectroscopy (SW-XPS).

In this article, I will briefly overview some of the early seminal work with SW-XPS, as pioneered by Yang and Fadley in the early 2000s [33–35], but then mainly focus on the latest state-of-the-art experimental and theoretical studies wherein standing-wave excitation is utilized to add depth-selectivity to well-established photoemission techniques, such as MCD, HAXPES, ARPES and PEEM. I will also discuss some of the more exotic X-ray optical effects, such as standing-wave localization and waveguides, that can be used in future studies to further enhance or suppress photoemission from specific layers within the sample.

2. Standing-wave photoemission

The field of standing-wave spectroscopy emerged with pioneering studies by Boris Batterman, who in 1964 first observed the formation of X-ray standing wave within a Ge crystal due to the Bragg reflection from the crystal planes [36]. It was furthermore reported that the resultant X-ray standing wave could be translated in the direction perpendicular to the diffracting crystal planes by changing the X-ray incidence angle through the Bragg condition. By doing so, and by simultaneously observing modulations in the intensities of core-level fluorescent X-rays as the standing wave swept through the crystal, one could accurately extract the positions of atoms near the surface of the sample. Following these early studies, standing wave spectroscopy has been applied extensively to investigate both the bulk crystal structure [37] as well as surface phenomena, such as reconstruction [38], formation of surface monolayers [39], and adsorbates [40].

All of the above-mentioned standing-wave experiments were naturally carried out in hard X-ray regime, which is well-suited for such crystallographic studies due to the sub-nanometer wavelengths. However, beginning with the works by Yang and Fadley [33–35] and by Kim and Kortright [41] a new type of depth-resolved photoemission technique was developed in which a standing wave was generated by a synthetic multilayer mirror with a periodicity on the order of several nanometers, thus allowing extending the standing-wave method into the soft X-ray regime.

As the first application of the soft X-ray standing-wave photoemission spectroscopy for the investigation of electronic structure of buried interfaces, Yang et al. used 750 eV soft X-ray radiation incident on a $[B_4C(22.5\,Å)/W(17.1\,Å)]_{40}$ periodic multilayer acting as a standing-wave generator [33]. The core-level photoelectron intensities of each element in the sample, including surface contaminant overlayers, were observed as a function of the incidence angle and therefore as a function of the vertical position of the standing wave within the sample. The resultant rocking-curve spectra were fitted using a specially written general-purpose program for calculating photoelectron, Auger electron, and X-ray emission intensities in the presence of all relevant X-ray optical effects, including excitation with standing-waves, absorption and multiple reflections at all interfaces, and total reflection at grazing incidence, as well as differential photoelectric subshell cross-sections, photoelectron inelastic mean-free paths, and refraction and internal reflection of the exiting photoelectron by the surface barrier. This program, termed YXRO for "Yang X-ray Optics", has recently been made available for general use [42] and has been thoroughly discussed in an extensive paper by Yang et al., which outlines all the theoretical components of the X-ray optical methodology [43]. Best fits to the experimental rocking curves for B, C, W and O core-level peaks yielded an Ångstrom-resolution element-resolved compositional depth profile of the sample, including thicknesses of all layers, chemical interdiffusion between them, and depth-resolved changes in the chemical state of C at the surface [33]. Thus, in this first proof-of-principle study, SW-XPS provided complete depth- and element-specific picture of a multilayer sample including chemical interdiffusion at the buried interface.

The only other technique capable of competing with SW-XPS, both in terms of depth resolution and element specificity, is cross-sectional scanning transmission electron microscopy (STEM) with electron energy loss spectroscopy (EELS) [44]. However, in contrast with SW-XPS, STEM-EELS does not easily allow access to various core-levels for the same element and cannot readily see element-specific magnetization – a powerful capability demonstrated in the second SW-XPS study in 2002 [35]. In addition to this, unlike STEM, SW-XPS is a non-destructive technique and does not require any sample preparation if carried out in the soft X-ray regime or at higher photon energies. Later in this article I will give an example of using STEM-EELS to confirm the results of a SW-XPS study and provide useful complimentary information about local roughness and chemical interdiffusion at a buried interface.

The standing-wave technique has several important limitations. In order to maximize the amplitude of the standing wave, a sample has to be grown as, or on top of, a synthetic superlattice. In case of the polycrystalline films this can be easily achieved by depositing a heterostructure of interest on top of the Mo/Si multilayer mirrors, which are now becoming ubiquitous in EUV lithography applications. For single-crystalline epitaxial systems, however, preparation of a high-quality sample which is optimal for SW-XPS can be difficult and in some cases impossible. For such systems the major challenge lies in growing a binary epitaxial superlattice consisting of tens of periods (repetitions) while preserving quality and uniformity of the individual layers and interfaces. In cases of heterojunctions for which synthesis of such high-quality superlattices proves to be challenging, a better-behaved epitaxial multilayer system could sometimes be used as a substrate for the bilayer of interest. In such cases, however, lattice mismatch between the multilayer substrate and the bottom layer may become a restricting factor. In the future studies, use of epitaxial seed layers and/or buffer layers may remedy this limitation for some epitaxial systems.

Please cite this article in press as: A.X. Gray, Future directions in standing-wave photoemission, J. Electron Spectrosc. Relat. Phenom. (2014), http://dx.doi.org/10.1016/j.elspec.2014.05.004

3. Probing magnetic properties at the buried interface with SW-MCD

In their first SW-XPS study Yang et al. suggested that the standing-wave technique could be utilized in conjunction with X-ray magnetic circular dichroism (SW-MCD) for depth-selective and element-specific determination of magnetic properties at buried interfaces [33,34]. Since then, several such studies have been carried out for heterojunctions of scientific and technological significance such as the Fe/Cr interface that exhibits giant magnetoresistance effect [35,45] and CoFeB/CoFe interface, which is of key significance for the magnetic tunnel junction (MTJ) structures [46]. These studies were vital for the development of the SW-MCD methodology and were the first examples of the utilization of the "SWedge" approach, wherein the bottom layer of the heterojunction is grown on top of the standing-wave generating multilayer mirror in a shape of a wedge with varying thickness. The SWedge allows one to scan the standing wave through the buried layers and interfaces without changing the X-ray incidence angle and/or photon energy but rather by moving the sample laterally along the x-direction. This method has an advantage over the "rocking-curve" technique used in the first SW study because it allows one to perform the experiment without deviating from the Bragg condition ($h\nu_{Bragg}$, θ_{Bragg}) so that maximum standing-wave intensity and a nearly identical phase of the wave with respect to the multilayer is always maintained [43]. In addition to using the SWedge method for scanning the standing-wave vertically across the buried interface between CoFeB and CoFe, the 2006 study [35] also demonstrated extension of the standing-wave photoemission beyond core-level spectroscopy and to the investigation of depth-selective valence-band electronic structure.

The latest SW-XPS and XW-MCD study by Yang et al. [47] utilized all of these methods to probe the electronic and magnetic properties of MgO/Fe interface, which is ubiquitous in the field of spintronics as one of the key building blocks for MTJs used in hard drive read heads and magnetic random access memory (MRAM). It was well known from theoretical calculations [48,49], as well as experimental studies [50,51], that a crystalline insulating MgO barrier enhances the tunneling magnetoresistance ratio (TMR) in an MTJ by selectively transmitting one spin orientation while filtering out the other due to specific wave function symmetries. However, the exact chemical, electronic, and magnetic structure of the MgO/Fe interface remained under debate. In particular, several questions critical to the device performance remained unanswered, such as (1) how the valence-band electronic structure and the insulating bandgap of MgO is changed by being in contact with the Fe layer, (2) whether Fe changes its chemical state/oxidizes at the interface with MgO, and (3) how the Fe magnetization decays in the interfacial region.

In order to address these questions, a heterojunction consisting of 10 Å of MgO on top of the Fe wedge with thickness varying continuously from 0 to 200 Å along the sample plane was grown on top of an 80-period $[Si/MoSi_2]_{80}$ multilayer mirror with the periodicity of 39.82 Å. The Fe layer was magnetized during growth with a small magnetic field (~300 G) applied along the transverse direction to the wedge corresponding to the easy axis. The sample was capped with a 12 Å layer of Al_2O_3 to protect the hydrophilic MgO layer against moisture contamination due to the exposure to ambient air. Measurements were carried out at the elliptically polarized undulator Beamline 4.0.2 at the Advanced Light Source (LBNL) with the photon energy fixed at 900 eV, which is well away from any absorption resonances, and by using *p*-polarized X-rays for all the wedge scans and circularly polarized light for the Fe SW-MCD scans. Finally, a strong X-ray standing wave was set-up within the sample by tuning into the 1st order Bragg condition for the $[Si/MoSi_2]_{80}$ multilayer, which occurs at the X-ray grazing incidence angle of $\theta_{Bragg} = 10.2^\circ$ at the photon energy of $h\nu_{Bragg} = 900$ eV. Sample structure and measurement geometry are schematically summarized in Fig. 1(a).

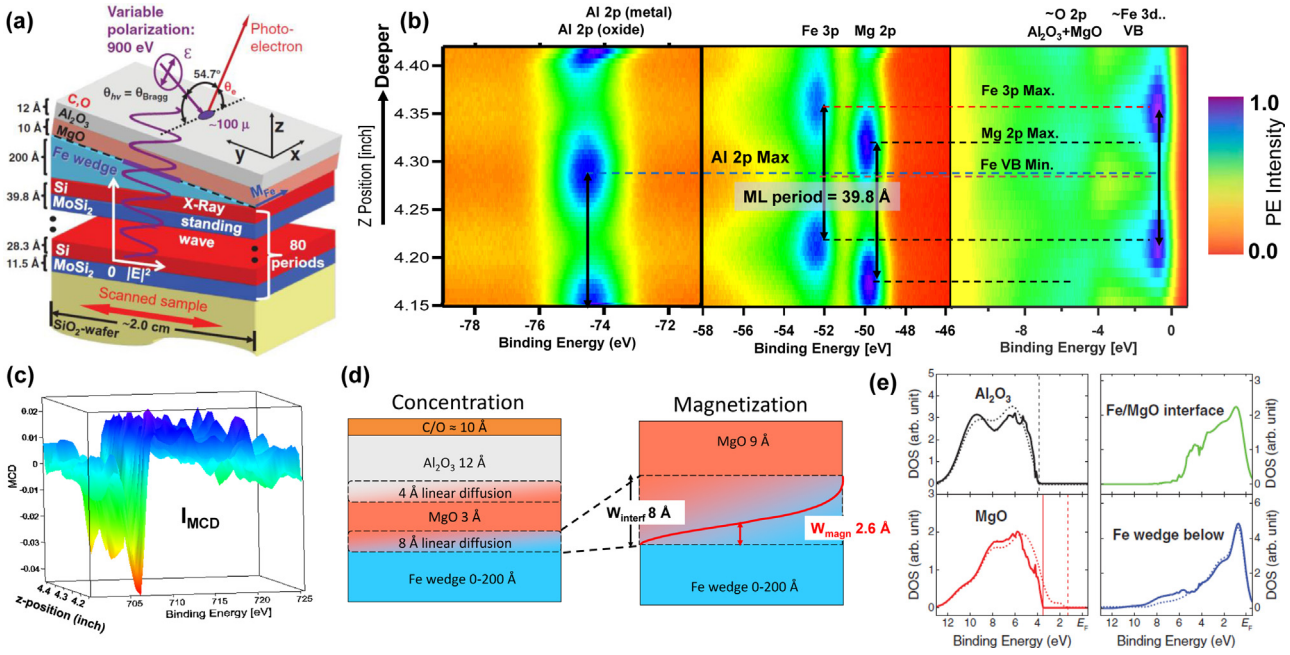

Fig. 1. (a) Schematic diagram of the sample, with the Fe in a wedge layer, and including the geometry of the exciting X-ray beam and outgoing photoelectrons. (b) 2D plots of the wedge scans of photoelectron spectra for Al 2*p* (left panel), Fe 3*p* and Mg 2*p* (middle panel), and the valence bands (right panel). (c) Fe 2*p* MCD signal derived from the photoemission intensity measurements taken in a wedge scan and with circularly polarized X-rays. (d) Final results for the concentration profile in the sample, including interdiffusion at all interface (left panel), and the atom-specific Fe magnetization across the Fe/MgO interface (right panel). (e) Layer-specific MEW-DOS for Al_2O_3, MgO, Fe/MgO interface, and Fe wedge layers extracted from the valence-band standing-wave data. Dotted curves represent the calculated MEW-DOS that do not take into account the interdiffused layer separately.

Source: From Ref. [47].

Please cite this article in press as: A.X. Gray, Future directions in standing-wave photoemission, J. Electron Spectrosc. Relat. Phenom. (2014), http://dx.doi.org/10.1016/j.elspec.2014.05.004

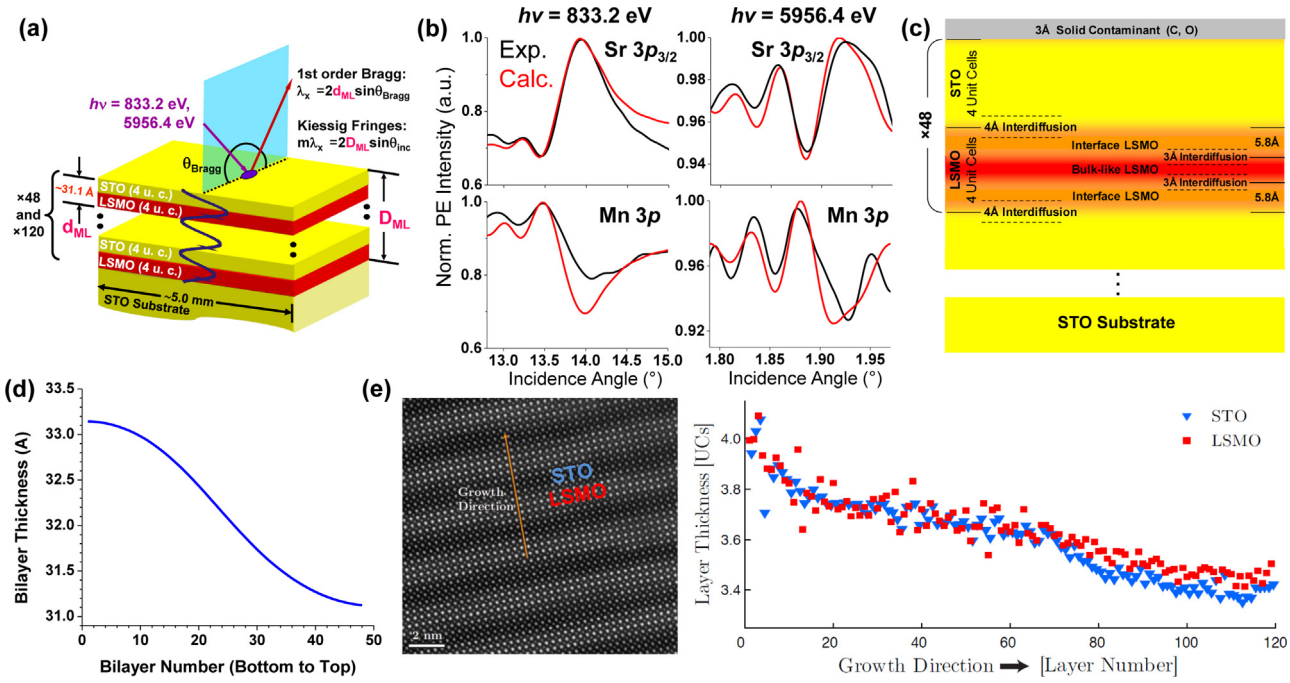

Fig. 2. (a) Schematics of the experimental geometry and the investigated multilayer structure consisting of 48 and 120 STO/LSMO bilayers grown epitaxially on a single-crystal STO substrate. (b) The best fits between the experimental and calculated rocking curves at 833.2 eV and 5956.4 eV for Sr $3p_{3/2}$ and Mn 3*p* core-level peaks. (c) Model of the sample which self-consistently describes the behavior of the rocking curves for every constituent element in the structure for both soft and hard X-ray regimes. (d) A 1 Å smooth bottom-to-top thickness gradient for the LSMO and STO layers in the superlattice, resulting from the rocking-curve analysis, and confirmed by a direct measurement using high-resolution cross-sectional STEM shown in (e).

Source: From Refs. [53,58].

Experimental SWedge scans of the photoemission spectra for Al 2*p*, Fe 3*p*, Mg 2*p* and the valence-band region are shown in Fig. 1(b) and exhibit strong (40–60%) modulations in intensity along the *z* position (lateral wedge scan direction) on the sample. Amplitude of the SW modulation provides a good quantitative measure of the depth-selective enhancement of the photoemission signal within the sample. Strikingly, even through visual comparison of the SW peak positions in the three panels of Fig. 1(b) one can easily identify the Fe-derived states in the valence-band manifold (right panel), by comparing their positions to the positions of the Fe core-level peaks in the middle panel. This remarkable observation suggests that SW-XPS can be used to extract depth-resolved matrix-element-weighted densities of states (MEW-DOS).

In addition to the core-level and valence-band SWedge scans shown in Fig. 1(b), Fe 2*p* photoemission MCD spectra were recorded for every *z* position along the wedge using circularly polarized X-rays, providing depth-resolved information about the local magnetic moment on the Fe atoms (see Fig. 1(c)).

Experimental SWedge scans shown in Fig. 1(b) and (c) were fitted to the X-ray optical theory using the YXRO program [42,43], with the final best fits yielding the chemical and magnetic profiles of the MgO/Fe interface, as shown in Fig. 1(d). Thicknesses of the MgO (9 Å) and Al_2O_3 (14 Å) layers were found to be close to nominal (10 Å and 12 Å respectively). However, the Fe/MgO and MgO/Al_2O_3 interfaces were found to be linearly interdiffused over total lengths of 8 Å and 4 Å, respectively. Best theoretical fit of the experimental MCD data further revealed that over the depth of the 8 Å interfacial layer between Fe and MgO the magnetization decays with a Gaussian profile with a half-width of 2.6 Å, suggesting presence of a 2–3 Å thick magnetically dead layer at the top of the interface. Layer-resolved decomposition of the valence-band spectra shown in Fig. 1(e) confirmed that the dead layer has the MEW-DOS similar to that of FeO, which is metallic yet non-magnetic. Finally, layer-resolved MEW-DOS of MgO showed remarkable differences when calculated with and without the interdiffusion region (red solid and dashed spectra in Fig. 1(e)), suggesting that interdiffusion at the interface effectively lowers the tunneling barrier for the injected Fe spins from ~3.5 eV to ~1.3 eV, consistent with the I–V tunneling transport measurements [52].

The MgO/Fe study by Yang et al. [47] established a powerful recipe for a "complete" depth-resolved standing-wave photoemission experiment, including Ångstrom-resolution determination of element-specific chemical and magnetic profile of a buried interface and the adjacent layers, and extraction of layer-resolved MEW-DOS never-before accessible via experimental techniques. Future works will likely extend this methodology to layer-selective spatially- and momentum-resolved studies of the valence-band structure, with some of these studies already starting to be carried out at synchrotron facilities around the world. In addition to this, new efficient spin-resolved photoemission techniques promise to play an important part in the future studies of spintronic materials and interfaces, and could be readily combined with the standing-wave approach. This development could be particularly useful for systems such as topological insulators, in which spin-resolved electronic structure exhibits significant variation between the interface and the bulk.

4. Probing electronic structure at the buried interface with resonant SW-XPS and SW-HAXPES

In another recent standing-wave photoemission study of the $La_{0.7}Sr_{0.3}MnO_3/SrTiO_3$ (LSMO/STO) MTJ interface Gray et al. have introduced two important advances to the standing-wave methodology that will undoubtedly be used in the future studies: (1) tuning the photon energy of the soft X-rays to the core-level resonance of one of the elements in the multilayer (La $3d_{3/2}$ in this case)

Please cite this article in press as: A.X. Gray, Future directions in standing-wave photoemission, J. Electron Spectrosc. Relat. Phenom. (2014), http://dx.doi.org/10.1016/j.elspec.2014.05.004

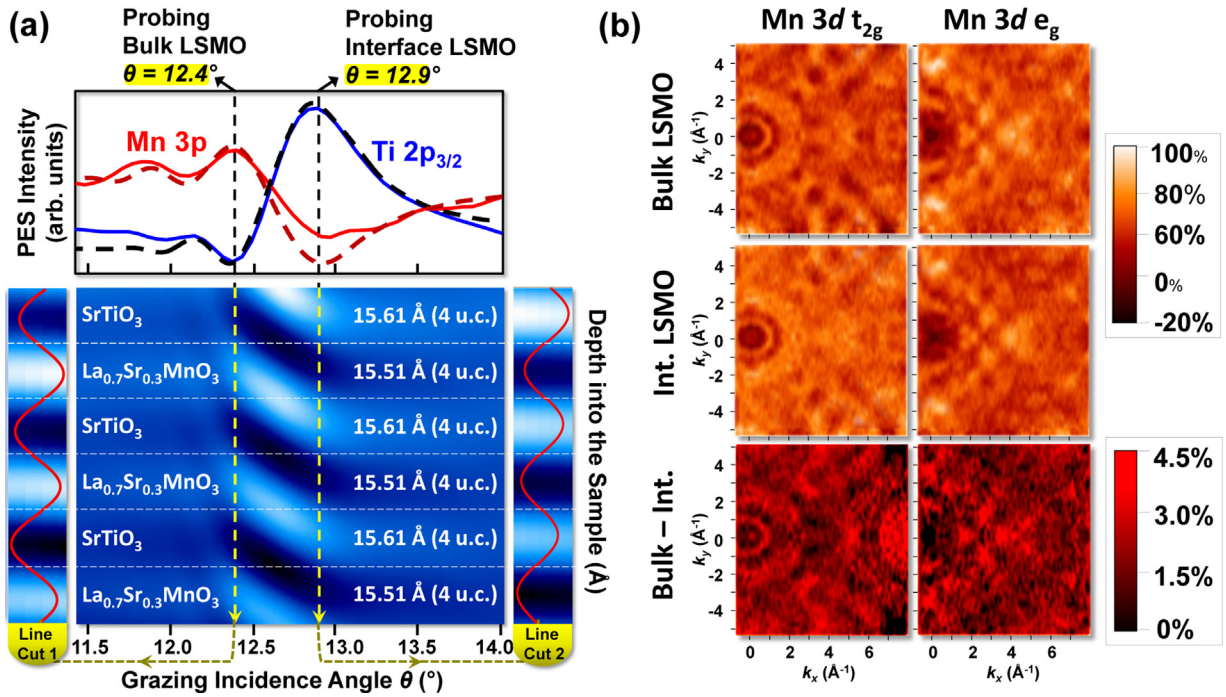

Fig. 3. (a) Simulated intensity of the X-ray standing-wave electric field (E^2) inside the sample as a function of depth and grazing incidence angle. The line cuts indicate that, for incidence angles <12.4°, the standing wave field highlights the bulk or center of the LSMO layer, but for angles >12.9° the interface regions of the LSMO layer are emphasized. The best fits of the experimental rocking-curves (top panel) for the Ti $2p_{3/2}$ and Mn 3*p* core-level peaks confirm the results of the simulation. (b) Angle-resolved (k_x, k_y) SWARPES intensity maps of the Mn 3*d* e_g and Mn 3*d* t_{2g} states obtained in the bulk-LSMO-sensitive and interface-LSMO-sensitive experimental geometries. Differences between the bulk- and interface-sensitive electronic structure are shown in the bottom panels.

Source: From Ref. [58].

in order to enhance the optical contrast between the alternating layers at that photon energy, thus maximizing the reflectivity and the standing-wave amplitude, and (2) combining soft X-ray standing wave photoemission (SW-XPS) with hard X-ray standing-wave photoemission (SW-HAXPES) with multi-keV excitation in order to enhance the probing depth by the virtue of increasing the IMFPs of photoemitted electrons [53]. It should be noted that around the same time, Döring et al. successfully applied SW-HAXPES to the investigation of buried interface between MgO and Fe [54].

The properties of the LSMO/STO/LSMO MTJ have been a subject of many detailed studies due to the recent theoretical prediction of the 100% TMR effect in this complex oxide heterojunction [55]. To date, however, maximum TMR effect realized in such MJT has been on the order of 80% [56] with a general consensus that such poor performance is due to highly ocalized electronic-structural phenomena at the LSMO/STO interface, the exact physical origin of which remain under debate [57]. In order to address this important technological problem epitaxial superlattice samples consisting of 48 and 120 bilayers of LSMO and STO, each nominally four unit cells thick (~15.5 Å), were fabricated on single-crystal STO substrates and investigated with both soft- and hard X-ray standing-wave photoemission (see Fig. 2(a)). Due to the constraints of the complex oxide epitaxy, the possibility of growing a SWedge-type sample was excluded. Therefore, the standing wave was moved vertically through the interfaces by varying the incidence angle around the superlattice Bragg condition (rocking-curve method) between 12.8° and 15.0° for the soft X-rays and between 1.79° and 1.97° for the hard X-rays. All the soft X-ray photoemission measurements were carried out at Beamline 7.0.1 of the Advanced Light Source (LBNL) at the photon energy of the La $3d_{3/2}$ absorption resonance (833.2 eV) in order to maximize the standing-wave contrast and with an overall energy resolution of ~300 eV. Hard X-ray measurements, on the other hand, were carried out at Beamline BL15XU of SPring-8 (Sayo, Japan) at the photon energy of 5956.4 eV, a choice yielding optimum energy resolution (~230 meV) and that is well away from any of the absorption edges in LSMO or STO.

Rocking curves for Sr $3p_{3/2}$, which is an electronic orbital for an element specific to the STO layer, and for Mn 3*p*, which in turn is specific only to the LSMO layer, and the best resulting fits to the X-ray optical calculations are shown in Fig. 2(b) for both soft and hard X-ray regimes (see ref. [53] for RCs of the remaining elements in the LSMO/STO junction: Ti $2p_{3/2}$, O 1*s*, La $4d_{5/2}$, La $3d_{5/2}$, and C 1*s* from the carbon-containing surface adsorbate layer). The final chemical profile of the LSMO/STO junction resulting from the simultaneous and self-consistent fitting of the rocking curves for every constituent element is shown in Fig. 2(c) and reveals ~4 Å of chemical interdiffusion between the LSMO and STO layers and altered optical constants of the LSMO layer at the interface with STO, consistent with the change in the Mn bonding at the interface. Furthermore, accurate fitting of the anomalously high relative amplitudes of the Kiessig fringes on both sides of the Bragg peak is only possible by assuming a 1 Å smooth bottom-to-top thickness gradient for the LSMO and STO layers in the superlattice, as shown in Fig. 2(d), a result which was later confirmed by a direct measurement using high-resolution cross-sectional STEM with both high-angle annular dark field (HAADF) and electron energy loss spectroscopy (EELS) (see Fig. 2(e) and [58]), and consistent with a slow decay of the laser intensity during the 6-or-more-hour-long pulsed laser deposition growth process. Thus, this study has demonstrated that in addition to determining chemical profile at a buried interface, resonant SW-XPS and SW-HAXPES can also be utilized for the investigation of Ångstrom-level changes in periodicity of superlattices over the depths of >1000 Å – a distance which is ~10–20 times longer than the characteristic IMFPs for photoelectrons in STO or LSMO in the hard X-ray regime [20,21].

Please cite this article in press as: A.X. Gray, Future directions in standing-wave photoemission, J. Electron Spectrosc. Relat. Phenom. (2014), http://dx.doi.org/10.1016/j.elspec.2014.05.004

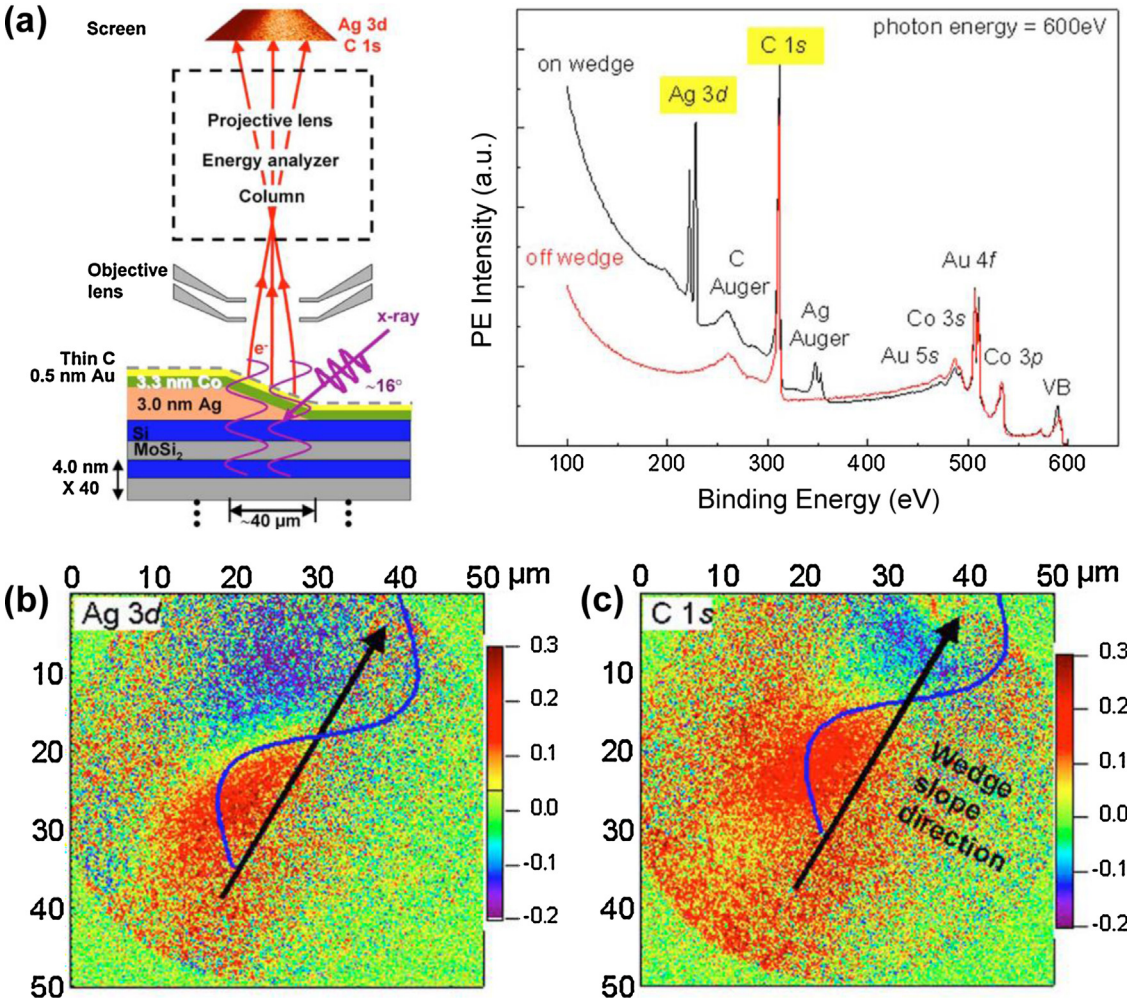

Fig. 4. (a) Schematics of the experimental SW-PEEM setup and the investigated SWedge sample as well as the typical broad binding-energy-range photoemission survey spectra from the sample obtained with the X-ray spot on and off the Ag wedge. Photoelectrons originating from the Ag 3*d* and C 1*s* core levels, which are highlighted in the figure, were used to image the sample. (b) and (c) Element-specific SW-PEEM images of the wedge part of the sample obtained by imaging via the Ag 3*d* and C 1*s* photoelectrons. The spatial phase shift observed between the two images is due to the different vertical positions of C and Ag layers with respect to the multilayer mirror which generates the standing wave.

Source: From Ref. [59].

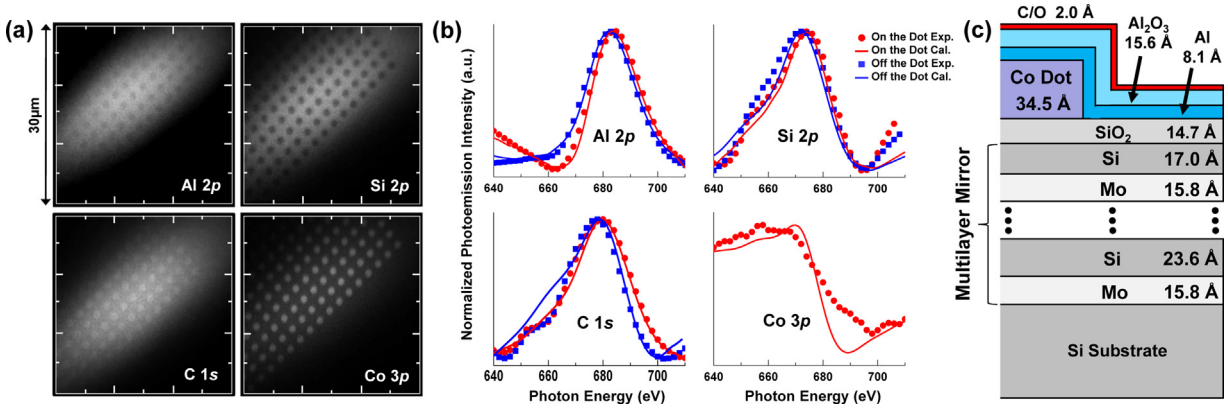

Fig. 5. (a) SW-PEEM images captured at $h\nu = 680$ eV, for Al 2*p*, C 1*s*, Si 2*p* and Co 3*p* core levels. (b) Experimental (data points) and calculated (solid curves) results of photoemission intensity as functions of photon energy with the electron kinetic energy for imaging set to the core-levels shown in (a). (c) Self-consistent model of the film structure obtained as the result of simultaneous fitting of all the scanned-energy curves in (b).

Source: From Ref. [60].

Please cite this article in press as: A.X. Gray, Future directions in standing-wave photoemission, J. Electron Spectrosc. Relat. Phenom. (2014), http://dx.doi.org/10.1016/j.elspec.2014.05.004

5. Probing momentum-resolved electronic structure at a buried interface with SWARPES

Finally, arguably the most sophisticated application of the standing-wave spectroscopy to date has been recently realized by combining SW-XPS with ARPES to devise a depth-selective technique for probing the *k*-resolved electronic structure of buried layers and interfaces – SWARPES [58]. The first proof-of-principle SWARPES study was carried out by Gray et al. on a LSMO/STO superlattice similar to the one discussed above, and was feasible due to the fact that with a detailed knowledge of the sample configuration and X-ray optical constants of the constituent layers, the electric-field intensity (E^2) profile of the standing wave inside the superlattice can be accurately modeled as a function of depth and incidence angle, as shown in Fig. 3(a). Thereupon, by fixing the X-ray incidence angle at the well-defined values determined by such simulations and confirmed by core-level rocking-curve measurements, one could accurately localize the standing-wave maxima either at the center ("bulk") region of the buried LSMO layer, or at the interface between LSMO and STO, as shown in the line-cuts in Fig. 3(a). Momentum-resolved ARPES measurements were then carried out in these two experimental geometries, yielding depth-selective three-dimensional photoelectron dispersions $E_B(k_x,k_y,(k_z))$ with k_z implicitly known but not directly measured. Constant-binding-energy "slices" of the (E_B,k_x,k_y) momentum space taken at the binding energies of the Mn 3*d* e_g and t_{2g} valence states (ca. −1.0 eV and −2.4 eV, respectively) are shown in Fig. 3(b) for the bulk-sensitive and interface-sensitive experimental geometries, and exhibit markedly different momentum dispersions. Finally, the bulk-minus-interface (k_x,k_y) maps shown in the bottom row of Fig. 3(b) indicate clear depth-dependent differences in electronic dispersion, suggesting a change in the Mn chemical state at the LSMO/STO interface.

SWARPES thus represents a powerful new technique for studying *k*-resolved valence-band electronic structure with true depth-selectivity [58]. Furthermore, since such depth-selectivity is achieved solely with X-ray optical effects within a multilayer sample, SWARPES measurements can therefore be readily carried out at any soft X-ray photoemission beamline equipped with a 2D photoelectron detector and a goniometer capable of rotating the sample around the polar axes. Thus, it is suggested that SWARPES method should be of broad application in the future depth-resolved studies of emergent phenomena at buried interfaces.

6. Adding depth resolution to photoemission microscopy with standing-wave excitation (SW-PEEM)

Addition of depth resolution to an existing technique which probes electronic structure in *momentum*-space (ARPES) prompts a question of whether the standing-wave method could be applied to a *real*-space microscopic imaging technique, such as photoemission microscopy (PEEM) [6–8]. PEEM has been used extensively in the past decade to investigate element-specific physical, chemical, and magnetic properties of surfaces by imaging the sample via photoexcitation of low-energy secondary electrons and/or core-level photoelectrons. However, prior to the advent of the standing-wave photoemission, PEEM has been inherently a lateral two-dimensional imaging technique. The possibility of extending the dimensionality of PEEM by adding depth resolution via standing-wave excitation has been recently demonstrated by Kronast et al. using the SWedge method [59]. In this proof-of-principle study, a narrow Ag wedge covered by a Au/Co bilayer and grown on top of a $(Si/Mo)_{40}$ multilayer mirror was imaged via element-specific core-level excitations from Ag 3*d* and C 1*s* subshells (see Fig. 4(a)). The need to scan the sample laterally along the wedge direction is eliminated since the resulting image is already inherently two-dimensional. Thus, core-level photoelectron intensities at the various lateral positions along the wedge direction originate from different depths below the surface, providing element-specific depth-resolved information which can be accessed by analyzing corresponding regions of interest in the image (see Fig. 4(b) and (c)). It is noteworthy that the *vertical* resolution in such SW-PEEM images approaches ~3–4 Å (about 1/10 of the SW period) and is thus almost two orders of magnitude better than the currently achievable *lateral* resolution of PEEM.

In the latest SW-PEEM study, as a prelude to future nanodevice imaging applications Gray et al. investigated a square lateral array of circular magnetic Co microdots patterned on top of the $(Si/Mo)_{40}$

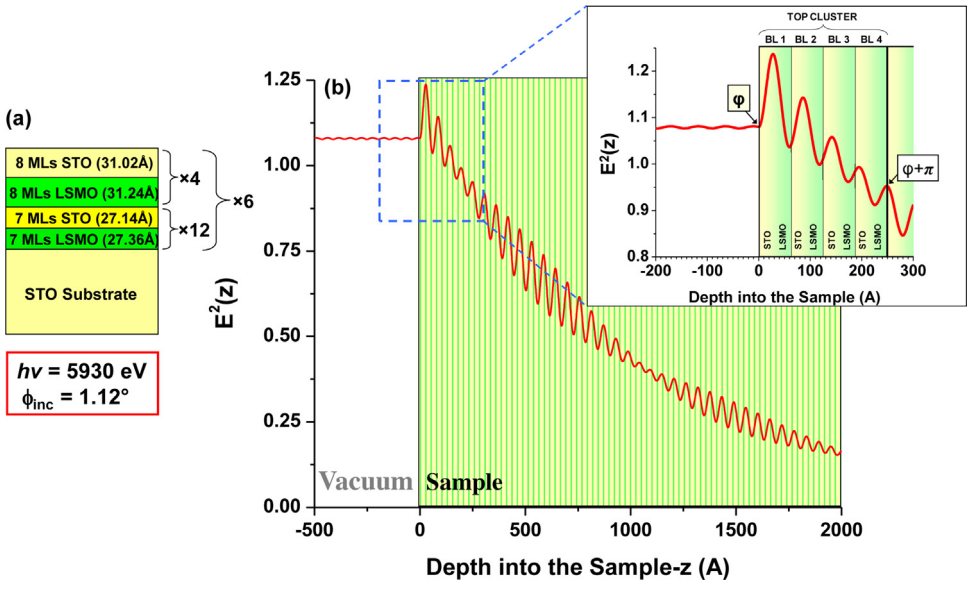

Fig. 6. (a) Schematic diagram of an aperiodic LSMO/STO multilayer structure which could be used for confining the standing wave within a sample. (b) Calculated X-ray electric-field intensity (E^2) versus sample depth for such aperiodic multilayer (at $h\nu = 5930$ eV, and $\phi_{inc} = 1.12^\circ$). At each cluster boundary the phase of the standing wave is always either delayed or advanced by π, as shown in the inset depicting the top bilayer cluster.
Source: From Ref. [43].

Please cite this article in press as: A.X. Gray, Future directions in standing-wave photoemission, J. Electron Spectrosc. Relat. Phenom. (2014), http://dx.doi.org/10.1016/j.elspec.2014.05.004

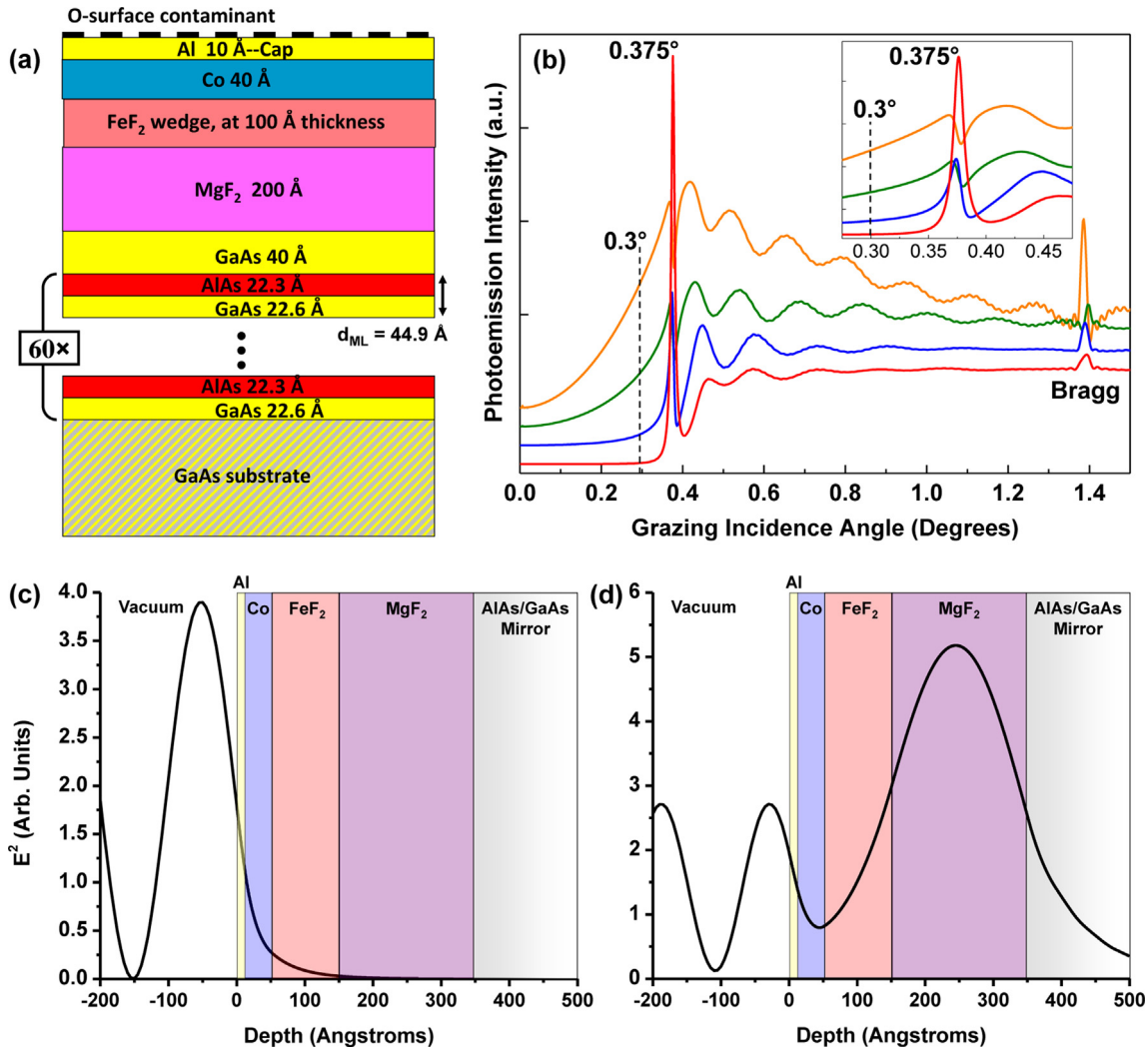

Fig. 7. (a) Schematic cross section of a typical sample which could be used to study interface phenomena in an exchange-bias junction. (b) Calculated photoemission intensities originating from various electronic subshells as functions of X-ray grazing incidence angle for typical hard X-ray photon energy of 5930 eV. (c) X-ray *E*-field intensity as a function of depth at a grazing incidence angle of 0.30°, where total reflection has begun to occur at the top Co surface, and (d) at a grazing incidence angle of 0.375°, where the waveguide effect is observed in the MgF_2 layer.

Source: From Ref. [43].

SW-generator multilayer and capped with a thin Al layer to prevent Co oxidation [60]. As a technical improvement upon the first study, vertical movement of the standing-wave through the structure was accomplished by means of varying the photon energy, which eliminated the need to grow the layer of interest in a shape of a wedge, thus opening the door for future three-dimensional measurements of more technologically relevant patterned structures and interfaces between epitaxial layers.

Results of the study are summarized in Fig. 5, including element-specific images of the sample obtained by core-level photoelectron imaging (Fig. 5(a)), experimental and calculated best-fit rocking curves of Al 2*p*, Si 2*p*, C 1*s* and Co 3*p* core-level photoemission intensities as a function of photon energy (Fig. 5(b)), and the resultant model of the structure's chemical profile (Fig. 5(c)). Excellent agreement between the experimental results and the calculations suggests that the photon-energy-scanning approach has a far-reaching potential for future Ångstrom-resolution depth-selective imaging studies of nanostructures. Finally, as an exciting possibility for the future, carrying out SW-PEEM experiments with varying circular and linear X-ray polarizations should introduce magnetic sensitivity into the technique, thus resulting in a new way of studying interface magnetism in spintronic devices.

7. Standing-wave localization, total reflection and waveguide effects

Looking ahead to future standing-wave photoemission studies, one can ask if there are ways to further localize and tailor the intensity of the X-ray electric field within a sample, thus achieving even more enhanced depth control. Several possible techniques for such standing-wave "focusing" have been recently proposed in a theoretical study by Yang et al. [43] and are summarized below.

One possible way of confining the standing wave within a sample is accomplished by the use of aperiodic multilayers consisting of two (or more) types of periodic superlattice clusters. An example of one such aperiodic structure, which is by no means unique, is depicted in Fig. 6(a). The proposed multilayer consists of two alternating superlattice clusters – (LSMO/STO) × 4 and (LSMO/STO) × 12, wherein each individual layer consists of 8 and 7 unit cells respectively. Standing-waves generated by these two intermixed clusters interfere within the total multilayer, creating a beat profile which is confined within the sample, as shown in Fig. 6(b) for the 5930 eV X-rays incident on the sample at 1.12° angle. As a result, the layer nearest to the surface exhibits the highest standing-wave modulation, while immediately above the

Please cite this article in press as: A.X. Gray, Future directions in standing-wave photoemission, J. Electron Spectrosc. Relat. Phenom. (2014), http://dx.doi.org/10.1016/j.elspec.2014.05.004

surface the standing-wave is almost non-existent. Such dramatic attenuation of the standing-wave intensity above the sample surface could potentially be useful for photoemission experiments probing solid-liquid and solid-gas interfaces.

Other methods take advantage of a rich variety of X-ray optical phenomena emerging in the region between the Bragg angle and the region of total external reflection. For example, an effective way of enhancing the surface sensitivity in a hard X-ray standing-wave photoemission experiment could be achieved by going to low grazing incidence angles, as realized in prior GIXPS/TRXPS studies [61,62]. An example of such near-surface enhancement is shown in Fig. 7, for a multilayer structure specifically designed for the studies of the interface phenomena in an exchange-bias junction Co/FeF_2 (Fig. 7(a)) [63]. As evident from the simulations in Fig. 7(b), for grazing incidence angles below 0.3° core-level photoemission intensities from the elements that comprise the deeper-lying layers, such as MgF_2 and FeF_2, are significantly reduced compared to those from the layers which are closer to the surface (Co and Al). Simulation of the electric-field intensity as a function of depth shown in Fig. 7(c) illustrates that at such low incidence angles (0.3° and lower) there is, in fact, very little *E*-field penetration below the surface of the sample, and thus most of the photoemission originates from the top Al and Co layers.

An even more striking effect is observed at the incidence angle of 0.375°, whereat a strong spike in the photoemission intensity from Mg 1*s* subshell is observed (see Fig. 7(b)). Such enhancement of photoemission from the MgF_2 layer can be explained by examining the *E*-field intensity profile inside the sample, as simulated in the plot shown in Fig. 7(d). Due to its low optical density, the MgF_2 layer acts as a waveguide, enhancing the *E*-field intensity within itself via multiple scattering of the X-rays from the top and bottom interfaces with the adjacent FeF_2 and AlAs layers which are more optically dense. Such waveguide effect has been recently observed experimentally in a hard X-ray fluorescence study of a Si/W/Si film structure, and was shown to provide a very effective method for *E*-field confinement with an enhanced sensitivity to the buried layer [64].

8. Concluding remarks

The ever-growing demand for miniaturization and increased speeds of next-generation electronic devices has taken experimental condensed matter physics to the quantum frontier in which emergent phenomena at the nanoscale require a clear differentiation between surface, bulk and interface properties. Thus, for many technologically promising novel materials, such as topological insulators, strongly correlated oxides and ferromagnetic semiconductors, electronic structure exhibits dramatic variation as a function of depth and proximity to other materials. Therefore, novel depth-resolved characterization techniques are required to disentangle these rich electronic behaviors, including magnetism and spin. Motivated by these challenges, in this article I have discussed several possible future directions in the field of photoemission, wherein powerful and well-established state-of-the-art spectroscopic and microscopic techniques, such as MCD, HAXPES, ARPES and PEEM, are combined with X-ray standing-wave excitation in order to achieve sub-nanometer-resolution depth-selectivity in the measurement. The future undoubtedly holds many more exciting developments in the field of standing-wave photoemission, with the imminent advances in the instrumentation and data analysis techniques leading to the addition of new dimensions, such as time and spin.

Acknowledgements

The work described in this article was supported by the Director, Office of Science, Office of Basic Energy Sciences, Materials Sciences and Engineering Division, of the U.S. Department of Energy under Contract Number DE-AC02-05CH11231, and by the Army Research Office MURI Program under Award W911-NF-09-1-0398. Research at Stanford was supported through the Stanford Institute for Materials and Energy Science (SIMES) and the LCLS by the US Department of Energy, Office of Basic Energy Sciences. The author would like to express special gratitude to Prof. C. S. Fadley (University of California, Davis and Lawrence Berkeley National Laboratory) for many fruitful discussions of all the studies mentioned in this overview. This work would also be impossible without tremendous contributions from the many collaborators of the Fadley Group.

References

[1] A. Einstein, Ann. Phys. 17 (1905) 132.
[2] C. Nordling, E. Sokolowski, K. Siegbahn, Phys. Rev. 105 (1957) 1676.
[3] K. Siegbahn, C. Nordling, A. Fahlman, K. Hamrin, J. Hedman, R. Nordberg, C. Johansson, T. Bergmark, S.-E. Karlsson, I. Lindgren, B. Lindberg, Atomic, Molecular and Solid-State Structure Studied by Means of Electron Spectroscopy, Nova Acta Regiae Soc. Sci. Ups. Almqvist and Wiksells, 1967, pp. 201–282.
[4] K. Siegbahn, C. Nordling, G. Johansson, J. Hedman, P.-F. Heden, K. Hamrin, U. Gelius, T. Bergmark, L.O. Werme, R. Manne, Y. Baer, North-Holland ESCA Applied to Free Molecules, The Netherlands, Amsterdam, 1969, pp. 200.
[5] I. Lindau, P. Pianetta, S. Doniach, W.E. Spicer, Nature 250 (1974) 214.
[6] S. Anders, H.A. Padmore, R.M. Duarte, T. Renner, T. Stammler, A. Scholl, M.R. Scheinfein, J. Stöhr, L. Séve, B. Sinkovic, Rev. Sci. Instrum. 70 (1999) 3973.
[7] E. Bauer, J. Electron Spectrosc. Relat. Phenom. 975 (2001) 114–116.
[8] C.M. Schneider, G. Schönhense, Rep. Prog. Phys. 65 (2002) 1785.
[9] A. Damascelli, Z. Hussain, Z.X. Shen, Rev. Mod. Phys. 75 (2003) 473.
[10] D.H. Lu, I.M. Vishik, M. Yi, Y. Chen, R.G. Moore, Z.X. Shen, Annu. Rev. Cond. Mat. Phys. 3 (2012) 129–167.
[11] B. Sinković, B. Hermsmeier, C.S. Fadley, Phys. Rev. Lett. 55 (1985) 1227.
[12] S. Thevuthasan, G.S. Herman, R.S. Saiki, A.P. Kaduwela, C.S. Fadley, Phys. Rev. Lett. 67 (1991) 469.
[13] G. Schütz, W. Wagner, W. Wilhelm, P. Kienle, R. Zeller, R. Frahm, G. Materlik, Phys. Rev. Lett. 58 (1987) 737.
[14] H.A. Dürr, G.Y. Guo, G. van der Laan, J. Lee, G. Lauhoff, J.A.C. Bland, Science 277 (1997) 213.
[15] J. Stöhr, A. Scholl, T.J. Regan, S. Anders, J. Lüning, M.R. Scheinfein, H.A. Padmore, R.L. White, Phys. Rev. Lett. 83 (1999) 1862.
[16] J.-H. Park, L.H. Tjeng, A. Tanaka, J.W. Allen, C.T. Chen, P. Metcalf, J.M. Honig, F.M.F. de Groot, G.A. Sawatzky, Phys. Rev. B 61 (2000) 11506.
[17] M.W. Haverkort, Z. Hu, A. Tanaka, W. Reichelt, S.V. Streltsov, M.A. Korotin, V.I. Anisimov, H.H. Hsieh, H.-J. Lin, C.T. Chen, D.I. Khomskii, L.H. Tjeng, Phys. Rev. Lett. 95 (2005) 196404.
[18] L.I. Johansson, J.W. Allen, T. Gustafsson, I. Lindau, S.B.M. Hagstrom, Solid State Commun. 28 (1978) 53.
[19] J.W. Allen, -J.S. Oh, I. Lindau, J.M. Lawrence, L.I. Johansson, S.B. Hagström, Phys. Rev. Lett. 46 (1981) 1100.
[20] C.J. Powell, A. Jablonski, I.S. Tilinin, S. Tanuma, D.R. Penn, J. Electron Spectrosc. Relat. Phenom. 98 (1999) 1.
[21] S. Tanuma, C.J. Powell, D.R. Penn, Surf. Interface Anal. 43 (2011) 689.
[22] T. Hara, M. Yabashi, T. Tanaka, T. Bizen, S. Goto, X.M. Marechal, T. Seike, K. Tamasaku, T. Ishikawa, H. Kitamura, Rev. Sci. Instrum. 73 (2002) 1125.
[23] H.A. Padmore, T. Warwick, J. Electron Spectrosc. Relat. Phenom. 75 (1995) 9.
[24] B. Wannberg, Nucl. Instrum. Methods Phys. Res. A 601 (2009) 182.
[25] Based on the TPP-2M IMFP calculations carried out for W at the photon energies of 50, 1500, 2000 and 15000 eV.
[26] C. Dallera, L. Duò, L. Braicovich, G. Panaccione, G. Paolicelli, B. Cowie, J. Zegenhagen, Appl. Phys. Lett. 85 (2004) 4532.
[27] Programs and abstract archives from two recent hard X-ray photoemission workshops (HAXPES 2011 and 2013): http://indico.desy.de/ConferenceDisplay.py?confId=3713 and http://www-conference.slu.se/haxpes2013/
[28] C. Wiemann, M. Patt, S. Cramm, M. Escher, M. Merkel, A. Gloskovskii, S. Thiess, W. Drube, C.M. Schneider, Appl. Phys. Lett. 100 (2012) 223106.
[29] A.X. Gray, C. Papp, S. Ueda, B. Balke, Y. Yamashita, L. Plucinski, J. Minár, J. Braun, E. Ylvisaker, C.M. Schneider, W.E. Pickett, H. Ebert, K. Kobayashi, C.S. Fadley, Nat. Mater. 10 (2011) 759.
[30] A.X. Gray, J. Minár, S. Ueda, P.R. Stone, Y. Yamashita, J. Fujii, J. Braun, L. Plucinski, C.M. Schneider, G. Panaccione, H. Ebert, O.D. Dubon, K. Kobayashi, C.S. Fadley, Nat. Mater. 11 (2012) 957.
[31] X. Kozina, G.H. Fecher, G. Stryganyuk, S. Ouardi, B. Balke, C. Felser, G. Schönhense, E. Ikenaga, T. Sugiyama, N. Kawamura, M. Suzuki, T. Taira, T. Uemura, M. Yamamoto, H. Sukegawa, W. Wang, K. Inomata, K. Kobayashi, Phys. Rev. B 84 (2011) 054449.
[32] C.S. Fadley, C.R. Brundle, in: A.D. Baker (Ed.), Electron Spectroscopy: Theory, Techniques, and Applications, Academic, London, 1978, Chap. 1, Vol. II.
[33] S.-H. Yang, B.S. Mun, A.W. Kay, S.-K. Kim, J.B. Kortright, J.H. Underwood, Z. Hussain, C.S. Fadley, Surf. Sci. Lett. 461 (2000) L557.
[34] S.-H. Yang, B.S. Mun, A.W. Kay, S.K. Kim, J.B. Kortright, J.H. Underwood, Z. Hussain, C.S. Fadley, J. Electron Spectrosc. 114 (2001) 1089.

Please cite this article in press as: A.X. Gray, Future directions in standing-wave photoemission, J. Electron Spectrosc. Relat. Phenom. (2014), http://dx.doi.org/10.1016/j.elspec.2014.05.004

[35] S.-H. Yang, B.S. Mun, N. Mannella, S.-K. Kim, J.B. Kortright, J. Underwood, F. Salmassi, E. Arenholz, A. Young, Z. Hussain, M.A. Van Hove, C.S. Fadley, J. Phys. Cond. Matt. 14 (2002) L406.
[36] B.W. Batterman, Phys. Rev. 133 (1964) A759.
[37] H. Stragier, J.O. Cross, J.J. Rehr, B. LI, C.E. Sorensen, J.C. Bouldin, Woicik, Phys. Rev. Lett. 69 (1992) 3064.
[38] J.C. Woicik, T. Kendelewicz, K.E. Miyano, P.L. Cowan, C.E. Bouldin, B.A. Karlin, P. Pianetta, W.E. Spicer, Phys. Rev. Lett. 68 (1992) 341.
[39] T. Kendelewicz, J.C. Woicik, K.E. Miyano, A. Herrera-Gomez, P.L. Cowan, B.A. Karlin, C.E. Bouldin, P. Pianetta, W.E. Spicer, Phys. Rev. B 46 (1992) 7276.
[40] B.N. Dev, G. Materlik, R.L. Johnson, W. Kranz, P. Funke, Surf. Sci. 178 (1986) 1.
[41] S.K. Kim, J.B. Kortright, Phys. Rev Lett. 86 (2001) 1347.
[42] See https://sites.google.com/a/lbl.gov/yxro/ for the downloadable YXRO computer program and the installation instructions.
[43] S.-H. Yang, A.X. Gray, A.M. Kaiser, B.S. Mun, B.C. Sell, J.B. Kortright, C.S. Fadley, J. Appl. Phys. 113 (2013) 073513.
[44] L. Samet, D. Imhoff, J.-L. Maurice, J.-P. Contour, A. Gloter, T. Manoubi, A. Fert, C. Colliex, Eur. Phys. J. B 34 (2003) 179.
[45] B.C. Sell, S.B. Ritchey, S.-H. Yang, S.S.P. Parkin, M. Watanabe, B.S. Mun, L. Plucinski, N. Mannella, A. Nambu, J. Guo, M.W. West, F. Salmassi, J.B. Kortright, C.S. Fadley, J. Appl. Phys. 103 (2008) 083515.
[46] S.-H. Yang, B.S. Mun, N. Mannella, A. Nambu, B.C. Sell, S.B. Ritchey, F. Salmassi, A. Shick, S.S.P. Parkin, C.S. Fadley, J. Phys. Condens. Matter. 18 (2006) L259.
[47] S.-H. Yang, B. Balke, C. Papp, S. Döring, U. Berges, L. Plucinski, C. Westphal, C.M. Schneider, S.S.P. Parkin, C.S. Fadley, Phys. Rev. B 84 (2011) 84410.
[48] W.H. Butler, X.G. Zhang, T.C. Schulthess, J.M. MacLaren, Phys. Rev. B 63 (2001) 054416.
[49] J. Mathon, A. Umerski, Phys. Rev. B 63 (2001) 220403.
[50] S.S.P. Parkin, C. Kaiser, A. Panchula, P.M. Rice, B. Hughes, M. Samant, S.-H. Yang, Nat. Mater. 3 (2004) 862.
[51] S. Yuasa, T. Nagahama, A. Fukushima, Y. Suzuki, K. Ando, Nat. Mater. 3 (2004) 868.
[52] P.G. Mather, J.C. Read, R.A. Buhrman, Phys. Rev. B 73 (2006) 205412.
[53] A.X. Gray, C. Papp, B. Balke, S.-H. Yang, M. Huijben, E. Rotenberg, A. Bostwick, S. Ueda, Y. Yamashita, K. Kobayashi, E.M. Gullikson, J.B. Kortright, F.M.F. DeGroot, G. Rijnders, D.H.A. Blank, R. Ramesh, C.S. Fadley, Phys. Rev. B 82 (2010) 205116.
[54] S. Döring, F. Schönbohm, U. Berges, R. Schreiber, D.E. Bürgler, C.M. Schneider, M. Gorgoi, F. Schäfers, C. Papp, B. Balke, C.S. Fadley, C. Westphal, Phys. Rev. B 83 (2011) 165444.
[55] J.H. Park, E. Vescoso, H.J. Kim, C. Kwon, R. Ramesh, T. Venkatesan, Nature 392 (1998) 794.
[56] (a) Y. Lu, X.W. Li, G.Q. Gong, G. Xiao, A. Gupta, P. Lecoeur, J.Z. Sun, Y.Y. Wang, V.P. Dravid, Phys. Rev. B 54 (1996) R8357;
(b) J. Sun, W. Gallagher, P. Duncombe, L. Krusin-Elbaum, R.A. Altman, A. Gupta, Y. Lu, G.Q. Gong, G. Xiao, Appl. Phys. Lett. 69 (1996) 3266;
(c) M. Viret, M. Drouet, J. Nassar, J.P. Contour, C. Fermon, A. Fert, Europhys. Lett. 39 (1997) 545.
[57] (a) M. Izumi, Y. Ogimoto, Y. Okimoto, T. Manako, P. Ahmet, K. Nakajima, T. Chikyow, M. Kawasaki, Y. Tokura, Phys. Rev. B 64 (2001) 064429;
(b) Y. Ogimoto, M. Izumi, A. Sawa, T. Manako, H. Sato, H. Akoh, M. Kawasaki, Y. Tokura, Jpn. J. Appl. Phys. 42 (2003) L369.
[58] A.X. Gray, J. Minár, L. Plucinski, M. Huijben, A. Bostwick, E. Rotenberg, S.-H. Yang, J. Braun, A. Winkelmann, G. Conti, D. Eiteneer, A. Rattanachata, A.A. Greer, J. Ciston, C. Ophus, G. Rijnders, D.H.A. Blank, D. Doennig, R. Pentcheva, J.B. Kortright, C.M. Schneider, H. Ebert, C.S. Fadley, Europhys. Lett. 104 (2013) 17004.
[59] F. Kronast, R. Ovsyannikov, A. Kaiser, C. Wiemann, S.-H. Yang, D.E. Bürgler, R. Schreiber, F. Salmassi, P. Fischer, H.A. Dürr, C.M. Schneider, W. Eberhardt, C.S. Fadley, Appl. Phys. Lett. 93 (2008) 243116.
[60] A.X. Gray, F. Kronast, C. Papp, S.-H. Yang, S. Cramm, I.P. Krug, F. Salmassi, E.M. Gullikson, D.L. Hilken, E.H. Anderson, P. Fischer, H.A. Dürr, C.M. Schneider, C.S. Fadley, Appl. Phys. Lett. 97 (2010) 062503.
[61] J. Chester, T. Jach, S. Thurgate, J. Vac. Sci. Technol. B 11 (1993) 1609.
[62] J. Kawai, S. Hayakawa, Y. Kitajima, K. Maeda, Y. Gohshi, J. Electron Spectrosc. Relat. Phenom. 76 (1995) 313.
[63] J. Nogues, I.K. Schuller, J. Magn. Magn. Matter. 192 (1999) 203.
[64] A. Gupta, N. Darowski, I. Zizak, C. Meneghini, G. Schumacher, A. Erko, Spectrochim. Acta 62 (2007) 622.

Please cite this article in press as: A.X. Gray, Future directions in standing-wave photoemission, J. Electron Spectrosc. Relat. Phenom. (2014), http://dx.doi.org/10.1016/j.elspec.2014.05.004